HOKKAIDO UNIVERSITY

Title	A technology demonstration of propagator matrix power method for calculation of electron velocity distribution functions in gas in long-term transient and succeeding equilibrium states under dc electric fields
Author(s)	Sugawara, Hirotake; Iwamoto, Hikaru
Citation	Japanese Journal of Applied Physics, 60(4), 046001 https://doi.org/10.35848/1347-4065/abe8a7
Issue Date	2021-03-09
Doc URL	https://hdl.handle.net/2115/84340
Rights	©2021 The Japan Society of Applied Physics
Rights(URL)	https://creativecommons.org/licenses/by-nc-nd/4.0/
Type	journal article
File Information	Sugawara-2021-JJAP-60(4)-046001-HUSCAP98146.pdf

Hokkaido University Collection of Scholarly and Academic Papers : HUSCAP

Jpn. J. Appl. Phys. **Regular Paper**

A technology demonstration of propagator matrix power method for calculation of electron velocity distribution functions in gas in long-term transient and succeeding equilibrium states under dc electric fields *

Hirotake SUGAWARA[1†] and Hikaru IWAMOTO[2]

[1] *Graduate School of Information Science and Technology, Hokkaido University, Sapporo 060-0814, Japan*

[2] *Department of Electronics and Information Engineering, Hokkaido University, Sapporo 060-0814, Japan*

A matrix-based calculation for the electron velocity distribution function (EVDF) in gas under dc electric field is demonstrated. The propagator matrix power method (PMPM) repeats squaring the propagator matrix $\mathbf{P}$ for its powers $\mathbf{P}^2$, $\mathbf{P}^4$, $\mathbf{P}^8$, $\mathbf{P}^{16}$, $\cdots$, up to a sufficient order of the power $\mathbf{P}^{2^S}$. $\mathbf{P}$ is a square matrix representing the change of EVDF due to the electron acceleration by electric field and the electron scattering by gas molecules in a time step Δt. With an initial EVDF $\mathbf{f}(t_0)$ in a form of column vector, a matrix product $\mathbf{P}^{2^S}\mathbf{f}(t_0)$ gives the EVDF at $t = t_0 + 2^S\Delta t$. The PMPM enables us to observe the EVDF relaxation in a logarithmic time scale with linear increase of the matrix squaring steps S. Features of the PMPM are discussed, and theoretically possible extensions to models under crossed electric and magnetic fields and ac electric field are investigated.

KEYWORDS: electron velocity distribution function, propagator, matrix power, long-term relaxation, equilibrium solution

1. Introduction

There is undiminished demand for calculation of the electron velocity distribution function (EVDF) as an essential property of gas discharges and plasmas, because many of the electron transport coefficients and rates of electron–molecule reactions are derived from the EVDF. The Boltzmann equation (BE) analyses[1,2] and Monte Carlo (MC) simulations[3,4] are traditional and well-established computational methods to obtain the EVDF. Nowadays, use of a prevailing BE solver[5] is convenient to obtain equilibrium EVDF under given reduced electric field E/N (E is electric field, and N is gas molecule number density). On the other hand, MC simulations are suitable for observation of transient EVDF to clarify the mechanism of electron swarm relaxation. However, MC calculations may be accompanied by statistical uncertainty and instability and the relaxation time is not easily predictable, for example, when the relaxation is slow at low E/N or the electron population decreases by electron attachment.

*Published source: Japanese Journal of Applied Physics Vol. 60, No. 4, 046001 (2021), IOP Publishing 2021-04-01, DOI: 10.35848/1347-4065/abe8a7

†E-mail: sugawara@ist.hokudai.ac.jp

In this paper, we perform a technology demonstration of a new matrix-based approach to the EVDF in temporal relaxation process. This numerical scheme named propagator matrix power method (PMPM) is based on a propagator method (PM),[6] which is a numerical scheme to solve the BE for the EVDF. Various PM schemes, including equilibrium-only and time-evolution types, have been developed for the EVDF in different modes; e.g., the EVDF in steady-state Townsend mode,[7–10] time-variant EVDF under rf[11–15] and impulse[16] electric fields, and the equilibrium EVDF in crossed dc electric and magnetic fields.[17,18] The present PMPM belongs to the time-evolution type. It is applied to transient EVDF under dc electric field,[19–26] and that in equilibrium[6] is also obtained as a result of sufficiently long relaxation. This calculation is, in a physical point of view, equivalent to that by the time-dependent multi-term BE analyses,[27,28] but the PM and PMPM do not need mathematically complicated series expansion of the EVDF required in the BE analyses. The main numerical scheme of the PMPM is only simple matrix squaring operations repeated for S times to obtain the 2^Sth power of the propagator matrix $\mathbf{P}$. $\mathbf{P}$ is composed to quantify the change of the EVDF in a time step Δt, and we can obtain the EVDF after $2^S\Delta t$ from $\mathbf{P}^{2^S}$.

The PMPM requires a huge memory capacity to operate a large matrix $\mathbf{P}$ depending on the resolution of the EVDF. On the other hand, the PMPM can cover an extremely long transient process. The present technology demonstration intends mainly to show the applicability of the PMPM principle because the calculation is restricted strongly by the currently available computational resources both in the memory capacity and the speed. However, this effort would be meaningful as foundation to utilize future computer architectures to be developed vigorously because the matrix multiplication is one of the most basic and general operations in both mathematics and computer science. Furthermore, the matrix expression of the propagator would enable us to analyze and interpret the characteristics of the EVDF relaxation process and the equilibrium EVDF on the basis of algebra. Features of the PMPM for the dc electric field model and theoretical possibility of extensions to other models are discussed.

2. Simulation model and configuration

2.1 Model and assumptions

A uniform dc electric field $\mathbf{E} = (E_x, E_y, E_z) = (-E, 0, 0)$ $(E > 0)$ is assumed in boundary-free real space. An electron velocity $\mathbf{v} = (v_x, v_y, v_z)$ may be represented in a manner of polar coordinate as (v, θ, ϕ) with relations $v_x = v\cos\theta$, $v_y = v\sin\theta\cos\phi$, and $v_z = v\sin\theta\sin\phi$, where $v = |\mathbf{v}| = (v_x^2 + v_y^2 + v_z^2)^{1/2}$, θ is the angle between $\mathbf{v}$ and the $+v_x$-direction, and ϕ is the azimuthal angle around the v_x-axis of velocity space.

We consider only binary collisions between electrons and gas molecules in the ground state for simplicity. We assume that the electron scattering is isotropic and the EVDF is axisymmetric around the v_x-axis. Because the EVDF is uniform for ϕ, we may consider the

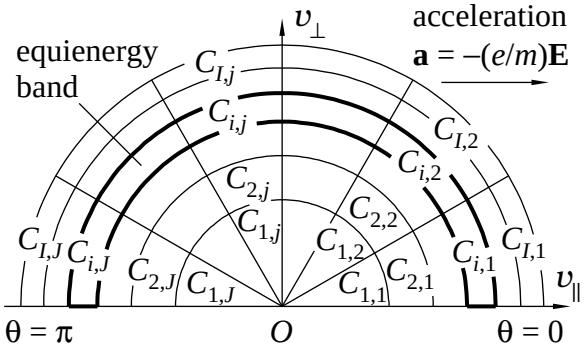

Fig. 1. Configuration of cells $C_{i,j}$ in velocity space. $v_{||} = v_x$ and $v_\perp = (v_y^2 + v_z^2)^{1/2}$ are, respectively, the velocity components parallel and perpendicular to $\mathbf{E}$. The region of $(i-1)\Delta\varepsilon \le \varepsilon < i\Delta\varepsilon$ surrounded by the thick curves represents an equienergy band, which corresponds to the ith submatrix $\mathbf{n}_i$ of the EVDF column vector $\mathbf{f}$.

EVDF in a two-variable form as $f(v,\theta)$. The calculation range for the EVDF is assumed as $0 \le v \le v_{\max}$ and $0 \le \theta \le \pi$. $v_{\max}$ is derived from a given maximum $\varepsilon_{\max}$ of the electron energy ε as $v_{\max} = v_{1\mathrm{eV}}(\varepsilon_{\max}/\varepsilon_{1\mathrm{eV}})^{1/2}$, where $\varepsilon_{1\mathrm{eV}} = 1\,\mathrm{eV}$ and $v_{1\mathrm{eV}}$ is the electron speed associated with 1 eV. $\varepsilon_{\max}$ is chosen so that we can effectively neglect the electrons with energies higher than $\varepsilon_{\max}$ in the EVDF.

2.2 Cells

Velocity space (v,θ) is partitioned into cells $C_{i,j}$ $(1 \le i \le I$ and $1 \le j \le J)$ as shown in Fig. 1. $C_{i,j}$ occupies the region of $v_{i-1} \le v < v_i$ and $\theta_{j-1} \le \theta < \theta_j$, where $v_i = v_{1\mathrm{eV}}(i\Delta\varepsilon/\varepsilon_{1\mathrm{eV}})^{1/2}$, $\Delta\varepsilon = \varepsilon_{\max}/I$, $\theta_j = j\Delta\theta$, and $\Delta\theta = \pi/J$. Here, v is sectioned with a constant $\Delta\varepsilon$ for convenience in the treatment of the energy loss at inelastic collisions.[6,9]

2.3 The EVDF in a vector form

Let $n_{i,j}$ be the number of electrons in $C_{i,j}$:

$$n_{i,j} = \int_{v=v_{i-1}}^{v_i} \int_{\theta=\theta_{j-1}}^{\theta_j} \int_{\phi=0}^{2\pi} f(v,\theta,\phi) v^2 \sin\theta \, dv d\theta d\phi. \tag{1}$$

The EVDF can be represented in a form of column vector $\mathbf{f}$ with a size of $IJ \times 1$ by arranging $n_{i,j}$ sequentially. We define $n_{i,j}$ as the $[(i-1)J+j]$th component of $\mathbf{f}$, then

$$\begin{aligned} \mathbf{f} &= \left(\mathbf{n}_1^{\mathrm{T}} \mid \mathbf{n}_2^{\mathrm{T}} \mid \cdots \mid \mathbf{n}_I^{\mathrm{T}}\right)^{\mathrm{T}} \\ &= \Big(\underbrace{n_{1,1}\ n_{1,2}\ \cdots\ n_{1,J}}_{0\le\varepsilon<\Delta\varepsilon} \mid \underbrace{n_{2,1}\ n_{2,2}\ \cdots\ n_{2,J}}_{\Delta\varepsilon\le\varepsilon<2\Delta\varepsilon} \mid \cdots \mid \\ &\qquad \underbrace{n_{I,1}\ n_{I,2}\ \cdots\ n_{I,J}}_{(I-1)\Delta\varepsilon\le\varepsilon<I\Delta\varepsilon} \Big)^{\mathrm{T}} \end{aligned} \tag{2}$$

$$\mathbf{n}_i = \left(n_{i,1}\ n_{i,2}\ \cdots\ n_{i,J} \right)^{\mathrm{T}} \tag{3}$$

$\mathbf{n}_i$ is a column vector with a size of $J \times 1$, and is the ith submatrix of $\mathbf{f}$ corresponding to the ith equienergy band depicted in Fig. 1.

The electron energy distribution function (EEDF) $F(\varepsilon)$ normalized by the electron population $n_\mathrm{e} = \sum_{i=1}^{I} \sum_{j=1}^{J} n_{i,j}$ is given as follows:

$$F(\varepsilon) = \frac{1}{n_\mathrm{e} \Delta\varepsilon} \sum_{j=1}^{J} n_{i,j} \quad \text{for } (i-1)\Delta\varepsilon \leq \varepsilon < i\Delta\varepsilon. \tag{4}$$

3. Propagator matrix power method

3.1 Propagator matrix

Let $\mathbf{P} = (p_{d,s})$ be the propagator matrix. $\mathbf{P}$ is a square matrix with a size of $IJ \times IJ$. With a given EVDF at time t_0, that at $t_0 + \Delta t$ is obtained as

$$\mathbf{f}(t_0 + \Delta t) = \mathbf{P}\mathbf{f}(t_0). \tag{5}$$

A component $p_{d,s}$ represents the ratio or probability of the electron transfer from a source cell $C_{i,j}$ (the sth cell, $s = (i-1)J + j$) to a destination cell $C_{i',j'}$ (the dth cell, $d = (i'-1)J + j'$) in a time step Δt induced by the change of $\mathbf{v}$ due to the electron acceleration by $\mathbf{E}$ and the scattering by gas molecules. The quantitative treatment of $p_{d,s}$ is presented later. Mathematically, $\mathbf{P}$ is called a stochastic or Markov matrix when the electron swarm is electron-conservative in the absence of ionization and electron attachment; $\mathbf{P}$ is a left stochastic matrix when $\sum_{d=1}^{IJ} p_{d,s} = 1$ for all s.

3.2 Principle of the PMPM calculation

A PM of time-evolution type calculates equation (5) step by step for every Δt. It can trace the physical relaxation process of the EVDF with a linear time progress. On the other hand, the PMPM calculates $\mathbf{P}^{2^S}$ by repeating matrix squaring operation as $\mathbf{P}$, $\mathbf{P}^2$, $\mathbf{P}^4$, $\mathbf{P}^8$, $\mathbf{P}^{16}$, $\cdots$, $\mathbf{P}^{2^S}$. Then, we can obtain the EVDF at $t_0 + 2^S\Delta t$ as

$$\mathbf{f}(t_0 + 2^S\Delta t) = \mathbf{P}^{2^S}\mathbf{f}(t_0). \tag{6}$$

It is interesting that $\mathbf{f}(t_0 + 2^S\Delta t)$ is obtained without calculating the halfway values of the EVDF in the period between t_0 and $t_0 + 2^S\Delta t$. The equilibrium EVDF is also available from equation (6) with a sufficiently large S corresponding to a long enough relaxation.

3.3 Construction of the propagator matrix

$\mathbf{P}$ is composed by the acceleration propagator matrix $\mathbf{P}_\mathrm{acc} = (a_{d,s})$ and the collision propagator matrix $\mathbf{P}_\mathrm{col} = (c_{d,s})$ as $\mathbf{P} = \mathbf{P}_\mathrm{acc}\mathbf{P}_\mathrm{col}$. $\mathbf{P}_\mathrm{acc}$ and $\mathbf{P}_\mathrm{col}$ are square matrices with a size of $IJ \times IJ$. They are constructed along Ref. 6 as outlined in the following steps, under a customization for the present configuration.

Step (a): All $c_{d,s}$ and $a_{d,s}$ are set at zero initially, and steps (b)–(e) are applied to all s from 1 to IJ.

Step (b): The ratios $r_{i,j}^{\mathrm{col,rem}}$ and $r_{i,j}^{\mathrm{acc,rem}}$ of the electrons to remain in $C_{i,j}$ respectively in the collision and acceleration processes are initially set at unity.

Step (c): The ratio $r_{i,j}^{\mathrm{col,out}}$ of the electrons to be scattered out of $C_{i,j}$ by collisions in Δt is subtracted from $r_{i,j}^{\mathrm{col,rem}}$ and added to $c_{d,s}$ specified by d of $C_{i',j'}$. $C_{i',j'}$ and $C_{i,j}$ are associated by the energy loss at collisions as explained in detail afterward.

Step (d): The ratio of the electrons flowing out of $C_{i,j}$ to the neighboring downstream destination cells $C_{i',j'}$ by the acceleration in Δt is subtracted from $r_{i,j}^{\mathrm{acc,rem}}$ and added to $a_{d,s}$ specified by d of $C_{i',j'}$.

Step (e): After redistributing all electron outflow from $C_{i,j}$, finally, $r_{i,j}^{\mathrm{col,rem}}$ and $r_{i,j}^{\mathrm{acc,rem}}$ are added (not substituted) respectively to $c_{s,s}$ and $a_{s,s}$; $c_{s,s}$ and $a_{s,s}$ may be already non-zero before this addition by the treatment in the preceding steps.

Both of $\mathbf{P}_{\mathrm{col}}$ and $\mathbf{P}_{\mathrm{acc}}$ represent the change of the EVDF in Δt, but the passage of time by the action of $\mathbf{P} = \mathbf{P}_{\mathrm{acc}}\mathbf{P}_{\mathrm{col}}$ is also Δt. This is interpreted as that the timing of collisions is discretized and the collisions are treated to be concentrated at the beginning of each time step Δt.

3.4 Details on collision propagator

In step (c), the ratio $r_{i,j}^{\mathrm{col,out}}$ of the electrons to be scattered out of $C_{i,j}$ by collisions is

$$r_{i,j}^{\mathrm{col,out}} = N q_{\mathrm{total}} v_i^{\mathrm{rep}} \Delta t = N \sum_k q_k v_i^{\mathrm{rep}} \Delta t, \tag{7}$$

where q_k is the cross section of the kth kind of collision of an ambient gas molecule, q_{total} is the total collision cross section, and v_i^{rep} is the representative electron speed of $C_{i,j}$ defined, for example, as

$$v_i^{\mathrm{rep}} = v_{1\mathrm{eV}} \sqrt{\frac{(i-1)\Delta\varepsilon + i\Delta\varepsilon}{2\varepsilon_{1\mathrm{eV}}}}. \tag{8}$$

$r_{i,j}^{\mathrm{col,out}}$ is subtracted from $r_{i,j}^{\mathrm{col,rem}}$. The breakdown of $r_{i,j}^{\mathrm{col,out}}$ for the kth kind of collision is $(q_k/q_{\mathrm{total}})r_{i,j}^{\mathrm{col,out}}$, and it is further distributed to $C_{i',j'}$ belonging to the specific equienergy bands determined by the energy loss of the kth kind of collision. The ratio that $C_{i',j'}$ receives is proportional to its solid angle $\Omega_{i',j'}$ subtended to the origin of velocity space under the assumption of isotropic scattering. $\Omega_{i',j'}$ is given as

$$\Omega_{i',j'} = \int_{\theta=\theta_{j'-1}}^{\theta_{j'}} \int_{\phi=0}^{2\pi} \sin\theta d\theta d\phi = 2\pi(\cos\theta_{j'-1} - \cos\theta_{j'}). \tag{9}$$

In case of elastic collisions, $C_{i,j}$ and $C_{i',j'}$ are regarded to belong to the same equienergy band ($i' = i$) because the electron energy is almost unchanged at an elastic collision. The ratio $r_{i',j'}^{\mathrm{col,in,elas}}$ to be added to $c_{d,s}$ is

$$r_{i',j'}^{\mathrm{col,in,elas}} = N q_{\mathrm{elas}} v_i^{\mathrm{rep}} \Delta t \frac{\Omega_{i',j'}}{4\pi}. \tag{10}$$

In case we need to consider the electron energy loss by the momentum transfer, a portion $(2m/M)(i'-1/2)r^{\mathrm{col,in,elas}}_{i',j'}$ is further replaced from $C_{i',j'}$ to $C_{i'-1,j'}$ for all j', where m/M is the mass ratio between an electron and a gas molecule.

In case of excitation collisions, $C_{i,j}$ and $C_{i',j'}$ are in a relation of $i' = i - l_{\mathrm{ex}}$, where $l_{\mathrm{ex}} = \lfloor \varepsilon_{\mathrm{ex}}/\Delta\varepsilon + 1/2 \rfloor$, $\varepsilon_{\mathrm{ex}}$ is the loss energy of the electron undergoing the excitation collision, and $\lfloor x + 1/2 \rfloor$ gives the integer closest to x. $r^{\mathrm{col,in,ex}}_{i',j'}$ to be added to $c_{d,s}$ is

$$r^{\mathrm{col,in,ex}}_{i',j'} = N q_{\mathrm{ex}} v_i^{\mathrm{rep}} \Delta t \frac{\Omega_{i',j'}}{4\pi}. \tag{11}$$

In case of ionization collisions, $C_{i,j}$ and $C_{i',j'}$ are in a relation of $i' \leq i - l_{\mathrm{ion}}$, where $l_{\mathrm{ion}} = \lfloor \varepsilon_{\mathrm{ion}}/\Delta\varepsilon + 1/2 \rfloor$, and $\varepsilon_{\mathrm{ion}}$ is the ionization potential. The energy division ratio between the primary and secondary electrons is assumed to be equiprobable from $0:1$ to $1:0$. At that time, the ratio added to $c_{d,s}$ is

$$r^{\mathrm{col,in,ion}}_{i',j'} = N q_{\mathrm{ion}} v_i^{\mathrm{rep}} \Delta t \delta_{i'} \frac{\Omega_{i',j'}}{4\pi}, \tag{12}$$

where $\delta_{i'}$ is the ratio of the redistribution of electrons corresponding to the equiprobable energy division:[6]

$$\delta_{i'} = \frac{4}{2(i - l_{\mathrm{ion}}) - 1} \quad \text{for } 1 \leq i' < i - l_{\mathrm{ion}}, \tag{13}$$

$$\delta_{i'} = \frac{2}{2(i - l_{\mathrm{ion}}) - 1} \quad \text{for } i' = i - l_{\mathrm{ion}}. \tag{14}$$

Here, $\sum_{i'=1}^{i-l_{\mathrm{ion}}} \delta_{i'} = 2$, which represents the primary and secondary electrons.

In case of electron attachment, the electrons undergoing attachment simply vanish. No ratio is added to $c_{d,s}$.

$\mathbf{P}_{\mathrm{col}}$ is a block upper triangular matrix:

$$\mathbf{P}_{\mathrm{col}} = \begin{pmatrix} \mathbf{C}_{1,1} & \mathbf{C}_{1,2} & \cdots & \mathbf{C}_{1,I-1} & \mathbf{C}_{1,I} \\ 0 & \mathbf{C}_{2,2} & \cdots & \mathbf{C}_{2,I-1} & \mathbf{C}_{2,I} \\ \vdots & \ddots & \ddots & \vdots & \vdots \\ \vdots & & \ddots & \mathbf{C}_{I-1,I-1} & \mathbf{C}_{I-1,I} \\ 0 & \cdots & \cdots & 0 & \mathbf{C}_{I,I} \end{pmatrix}, \tag{15}$$

where $\mathbf{C}_{i'',j''}$ is a $J \times J$ submatrix of $\mathbf{P}_{\mathrm{col}}$. $\mathbf{C}_{i'',j''}$ represents the re-distribution of electrons from source cells $C_{i,j}$ ($i = j''$, $1 \leq j \leq J$) in the j''th equienergy band to destination cells $C_{i',j'}$ ($i' = i''$, $1 \leq j' \leq J$) in the i''th equienergy band. $\mathbf{C}_{i'',j''} = 0$ for $i'' > j''$ represents that no energy increase occurs by the collisions mentioned above.

In case super-elastic collision is introduced to consider the influence of excited species, non-zero $\mathbf{C}_{i'',j''}$ may appear for such $i'' > j''$ that q_k for the super-elastic collision is non-zero in $(j''-1)\Delta\varepsilon \leq \varepsilon < j''\Delta\varepsilon$ and the electron energy increase is $(i''-j'')\Delta\varepsilon$. The number of electrons obtaining energy over $\varepsilon_{\max}$ should be negligible.

3.5 Details on acceleration propagator

In step (d), $C_{i,j}$ has two downstream neighbors, but either or both of them may be missing at the verge of the calculation range of velocity space. The downstream is the right in Fig. 1. The downstream neighbors of $C_{i,j}$ are $C_{i,j-1}$ for $j > 1$ and $C_{i+1,j}$ for $i < I$ when $1 \leq j \leq J/2$, and are $C_{i,j-1}$ for $j > 1$ and $C_{i-1,j}$ for $i > 1$ when $J/2 < j \leq J$. The ratio $r_{i,j}^{\mathrm{acc,out}}$ of the electrons to be transferred to the neighboring downstream cells is quantified as

$$r_{i,j}^{\mathrm{acc,out}} = \frac{S_{i,j}}{V_{i,j}} a\Delta t, \tag{16}$$

where $V_{i,j}$ is the volume of $C_{i,j}$, $S_{i,j}$ is the area of $C_{i,j}$ projected to a plane normal to the direction of the electron acceleration vector $\mathbf{a} = -(e/m)\mathbf{E}$, $a = |\mathbf{a}| = (e/m)E$ is the scaler electron acceleration by $\mathbf{E}$, and e and m are the electronic charge and mass, respectively. $S_{i,j}$ is $S_{i,j}^{-\theta} + S_{i,j}^{+\varepsilon}$ for $1 \leq j \leq J/2$, and $S_{i,j}^{-\theta} + S_{i,j}^{-\varepsilon}$ for $J/2 < j \leq J$. $S_{i,j}^{-\theta}$ is the projected area of the boundary between $C_{i,j}$ and $C_{i,j-1}$, and $S_{i,j}^{\pm\varepsilon}$ are those between $C_{i,j}$ and $C_{i\pm1,j}$:

$$\begin{aligned}
V_{i,j} &= \int_{v=v_{i-1}}^{v_i} \int_{\theta=\theta_{j-1}}^{\theta_j} \int_{\phi=0}^{2\pi} v^2 \sin\theta dv d\theta d\phi \\
&= \frac{2}{3}\pi(v_i^3 - v_{i-1}^3)(\cos\theta_{j-1} - \cos\theta_j), && (17) \\
S_{i,j}^{-\theta} &= \pi(v_i^2 - v_{i-1}^2)\sin^2\theta_{j-1}, && (18) \\
S_{i,j}^{+\varepsilon} &= \pi v_i^2(\sin^2\theta_j - \sin^2\theta_{j-1}), && (19) \\
S_{i,j}^{-\varepsilon} &= \pi v_{i-1}^2(\sin^2\theta_{j-1} - \sin^2\theta_j). && (20)
\end{aligned}$$

The ratio given to $C_{i,j-1}$ and $C_{i\pm1,j}$ are

$$\begin{aligned}
r_{i',j'}^{\mathrm{acc,in}} &= \frac{S_{i,j}^{-\theta}}{V_{i,j}} a\Delta t \quad \text{for } C_{i',j'} \equiv C_{i,j-1}, && (21) \\
r_{i',j'}^{\mathrm{acc,in}} &= \frac{S_{i,j}^{\pm\varepsilon}}{V_{i,j}} a\Delta t \quad \text{for } C_{i',j'} \equiv C_{i\pm1,j}. && (22)
\end{aligned}$$

$\mathbf{P}_{\mathrm{acc}}$ is in a block banded form:

$$\mathbf{P}_{\mathrm{acc}} = \begin{pmatrix}
\mathbf{A}_{1,1} & \mathbf{A}_{1,2} & 0 & \cdots & 0 \\
\mathbf{A}_{2,1} & \mathbf{A}_{2,2} & \ddots & \ddots & \vdots \\
0 & \ddots & \ddots & \ddots & 0 \\
\vdots & \ddots & \ddots & \mathbf{A}_{I-1,I-1} & \mathbf{A}_{I-1,I} \\
0 & \cdots & 0 & \mathbf{A}_{I,I-1} & \mathbf{A}_{I,I}
\end{pmatrix}, \tag{23}$$

where $\mathbf{A}_{i'',j''}$ is a $J \times J$ submatrix of $\mathbf{P}_{\mathrm{acc}}$ and $\mathbf{A}_{i'',j''} = 0$ for $i'' > j'' + 1$ and $i'' < j'' - 1$. The lower off-diagonal submatrices of $i'' = j'' + 1$ represent the energy increase by acceleration. They have non-zero components corresponding to the electron transfer from $C_{i,j}$ to $C_{i',j'} \equiv C_{i+1,j}$ for $1 \leq j \leq J/2$. The upper off-diagonal submatrices of $i'' = j'' - 1$ correspond to the electron deceleration in the electron transfer from $C_{i,j}$ to $C_{i',j'} \equiv C_{i-1,j}$ for $J/2 < j \leq J$.

3.6 Restrictions on the time step and relaxation time

There is a restriction for Δt under a chosen set of $\varepsilon_{\max}$, $\Delta\varepsilon$, and $\Delta\theta$. To avoid negative $r_{i,j}^{\mathrm{col,rem}}$ and $r_{i,j}^{\mathrm{acc,rem}}$, Δt must satisfy

$$r_{i,j}^{\mathrm{col,out}} = N q_{\mathrm{total}} v_i^{\mathrm{rep}} \Delta t \leq 1, \tag{24}$$

$$r_{i,j}^{\mathrm{acc,out}} = \frac{S_{i,j}}{V_{i,j}} a \Delta t \leq 1. \tag{25}$$

In most cases, these criteria can be tested with the properties of the thinnest cell $C_{I,J}$ because $r_{i,j}^{\mathrm{acc,out}}$ is dominant at low pressures.

$\mathbf{P} = \mathbf{P}_{\mathrm{acc}}\mathbf{P}_{\mathrm{col}}$ is in a block upper Hessenberg form as

$$\mathbf{P} = \begin{pmatrix} \mathbf{P'}_{1,1} & \mathbf{P'}_{1,2} & \cdots & \mathbf{P'}_{1,I-1} & \mathbf{P'}_{1,I} \\ \mathbf{P'}_{2,1} & \mathbf{P'}_{2,2} & \cdots & \mathbf{P'}_{2,I-1} & \mathbf{P'}_{2,I} \\ 0 & \ddots & & \vdots & \vdots \\ \vdots & \ddots & \ddots & \mathbf{P'}_{I-1,I-1} & \mathbf{P'}_{I-1,I} \\ 0 & \cdots & 0 & \mathbf{P'}_{I,I-1} & \mathbf{P'}_{I,I} \end{pmatrix}, \tag{26}$$

where $\mathbf{P'}_{i'',j''}$ is a $J \times J$ submatrix of $\mathbf{P}$, and $\mathbf{P'}_{i'',j''} = 0$ for $i'' > j'' + 1$ when super-elastic collision is not considered. This implies that the electron transfer from lower-ε cells to higher-ε cells in Δt is limited to be those between neighboring equienergy bands because the variation of $\mathbf{v}$ by acceleration is continuous. Thus, the relaxation to obtain the equilibrium EVDF requires $2^S \gg I$ in order that even the initial electrons in the equienergy band of the lowest ε diffuse over the cells. At the same time, the number of squaring operations S would have an upper limit as well in practical calculation to avoid overflow or underflow of components of $\mathbf{P}^{2^S}$. This is because the growth of the electron population n_{e} is superexponential with linear increase of S when the electrons are non-conservative in the presence of ionization and/or electron attachment. In equilibrium, we may assume

$$n_{\mathrm{e}} \propto \exp(\bar{\nu}_{\mathrm{ion}} t) = \exp(\bar{\nu}_{\mathrm{ion}} 2^S \Delta t), \tag{27}$$

where $\bar{\nu}_{\mathrm{ion}}$ is the effective ionization frequency. n_{e} grows or decays exponentially with t, and t proceeds exponentially with S. A low-resolution short test run would help a rough estimation of $\bar{\nu}_{\mathrm{ion}}$ to choose an appropriate upper limit $S_{\max}$ for S.

4. Demonstration

4.1 Computational facility and algorithm

The present demonstrations of the PMPM were performed by a workstation with the following properties: CPU, Intel Xeon W-2135 (3.7 GHz, 6-core); main memory, 32 GiB; operating system, Linux CentOS 7.3; programming language, C++. The memory capacity is sufficient for the chosen matrix size mentioned in §4.3.

The computational load of the PMPM increases rapidly if finer resolutions are required for

ε and θ. With the number of cells $n = IJ$, the order of the computational load $O(n^\omega)$, which is effectively determined by the number of scaler multiplications between the matrix components, is $\omega = 3$ in case the matrix squaring operation is performed in the way of the definition of the matrix multiplication. Efforts to reduce ω have been reported; $\omega = \log_2 7 \approx 2.807$ by Strassen's algorithm,[29] and $\omega \approx 2.376$ by the Coppersmith–Winograd algorithm.[30] ω has been lowered progressively to $\omega < 2.3736897$[31,32] and $\omega < 2.3728639$,[33] but the scheme becomes much complicated. Although a drastic shortening of the computational time is expected by utilizing some system-dependent matrix operation library, the present PMPM is performed with one of the simplest definition-based scheme commonly available for investigators.

A simple matrix squaring operation needs two arrays for $\mathbf{P}^{2^S}$ and $\mathbf{P}^{2^{S+1}}$. When $\mathbf{P}^{2^S}$ is given in array 1, $\mathbf{P}^{2^{S+1}}$ is obtained in array 2. After this, array 1 can be overwritten with $\mathbf{P}^{2^{S+2}}$. We do not need to restuff the latest $\mathbf{P}^{2^S}$ into array 1 every time, and thus a couple of matrix squaring operations become an iteration cycle.

4.2 Ambient gases and electric field

The EVDF is calculated for Ar at $E/N = 50$, 100, and 200 Td and a ramp model gas[34] at 1, 12, and 24 Td ($1\,\mathrm{Td} = 10^{-21}\,\mathrm{Vm}^2$). $N = 3.54 \times 10^{22}\,\mathrm{m}^{-3}$. Ar is a typical test gas, and this E/N value is an example of ionization-dominated case. The electron collision cross sections of Ar are taken from Ref. 35. The ramp model gas has often been used for benchmarks between different simulation methods and data for comparison are available from Refs. 36 and 37. It has a constant elastic collision cross section $q_{\mathrm{el}} = 6.0 \times 10^{-20}\,\mathrm{m}^2$ and an inelastic collision cross section q_{inel} defined as a ramp function of ε with a threshold and loss energy of 0.2 eV as $q_{\mathrm{inel}} = 10.0 \times 10^{-20} \times \max(0, \varepsilon/\varepsilon_{1\mathrm{eV}} - 0.2)\,\mathrm{m}^2$, where the max function gives the greatest value in the arguments.

4.3 Cell resolution and initial condition

We set $I = 1000$ and $J = 18$; i.e. 18 000 cells for the EVDF. $\mathbf{P}$ is an $18\,000 \times 18\,000$ matrix, which needs about 2.41 GiB to be allocated as a double-precision array.

$\varepsilon_{\max}$ is chosen to be 100 eV for Ar and 0.5, 2.5, and 10.0 eV for the ramp model gas at 1, 12, and 24 Td, respectively. Δt is set at 1 ps commonly. The squaring operation for $\mathbf{P}^{2^S}$ is repeated up to $S = S_{\max} = 20$ for Ar (the relaxation time is $2^{20}\Delta t \approx 1.05\,\mu\mathrm{s}$) and up to $S_{\max} = 30$ for the ramp model gas ($2^{30}\Delta t \approx 1.07$ ms) to cover the post-relaxation period longer than needed for reaching equilibrium.

The initial EVDF is formally assumed as the initial electrons are all in the cells of the lowest ε:

$$\mathbf{n}_1 = (\,1\;1\;\cdots\;1\,)^{\mathrm{T}}, \tag{28}$$

$$\mathbf{n}_i = (\,0\;0\;\cdots\;0\,)^{\mathrm{T}} \quad \text{for } 2 \le i \le I. \tag{29}$$

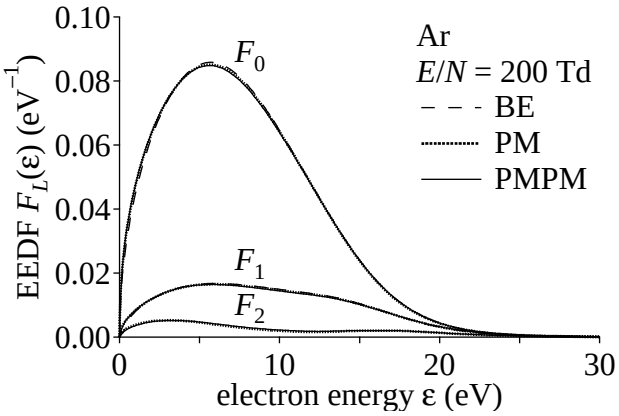

Fig. 2. EEDFs $F_L(\varepsilon)$ ($L = 0, 1, 2$) in Ar at $E/N = 200$ Td calculated by a BE (2-term approximation), an equilibrium-only PM, and the PMPM.

4.4 Results of equilibrium EEDF

The EEDF $F_L(\varepsilon)$ ($L = 0, 1, 2$) by the PMPM obtained from $\mathbf{P}^{2^{20}}\mathbf{f}(t_0)$ for Ar and $\mathbf{P}^{2^{30}}\mathbf{f}(t_0)$ for the ramp model gas are shown in Figs. 2 and 3 together with those in equilibrium calculated by a 2-term approximation of the BE analysis and an equilibrium-only PM.[6] F_0 ($= F(\varepsilon)$), F_1, and F_2 are the zeroth-, first-, and second-order Legendre spherical harmonics expansion terms of the EEDF, respectively. The BE results do not have F_2. Note that the expansion is not necessary in the PM and PMPM calculations, and it was done only for comparison with the BE results. $F(\varepsilon)$ is also shown in a form of the electron energy probability function (EEPF) $F(\varepsilon)/\sqrt{\varepsilon}$ in Fig. 4 to observe the decay of its high-ε tail. The discrepancy of the BE results at higher E/N and ε is due to insufficiency of the 2-term approximation for distorted EVDFs. The validity of the principle and implementation of the PMPM is verified by the agreement of the EEDFs and the EEPFs with the PM results.

The equilibrium-only methods took a few seconds for calculation. The PMPM took about 73–90 min for one squaring operation for an $18\,000 \times 18\,000$ matrix in early and late squaring steps, and this computational time per step temporarily increased up to 147 min in several midway steps in which the relaxation of the EVDF proceeds.

4.5 Results of relaxation process

The relaxation processes of the mean electron energy $\langle\varepsilon\rangle$ and the EEDF in the ramp model gas are presented in Figs. 5 and 6, respectively. The EEDFs at $S = 18$–20 in Fig. 6 are effectively identical to F_0 in Fig. 3. $\langle\varepsilon\rangle$ reaches its equilibrium value by $S = 20$ even in the slowest case. We see that the relaxation time may differ one or two orders of magnitude depending on E/N. However the relaxation time is long, $2^S\Delta t$ would eventually exceed it with linear increment of S. The PMPM can cover a wide range of relaxation time with a relatively small $S_{\max}$; i.e., one order of magnitude can be covered by four times of squaring

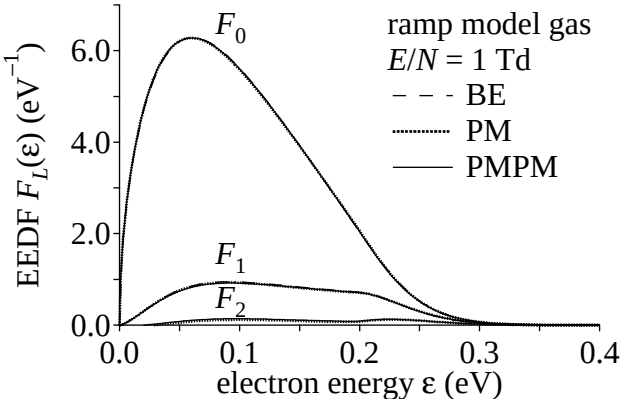

Fig. 3. EEDFs $F_L(\varepsilon)$ ($L = 0, 1, 2$) in the ramp model gas at $E/N = 1$ Td calculated by a BE (2-term approximation), an equilibrium-only PM, and the PMPM.

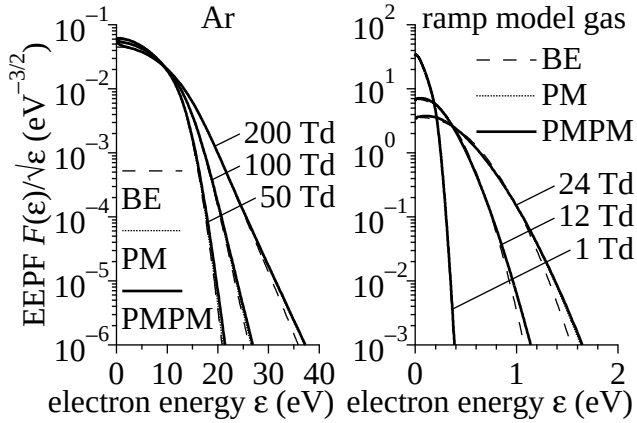

Fig. 4. EEPFs in Ar at $E/N = 50$, 100, and 200 Td and the ramp model gas at $E/N = 1$, 12, and 24 Td calculated by a BE (2-term approximation), an equilibrium-only PM, and the PMPM.

operations ($2^4 = 16 > 10$). The final phase of the relaxation, which is often trailed long, suddenly ends and a sufficiently large $S_{\max}$ to obtain equilibrium solution is found clearly because the progress of time expanding exponentially with S lets the final relaxation phase complete within a few times of squaring operations. This would make the runtime detection of the achievement of the EVDF relaxation easy.

When a specific relaxation time $k\Delta t$ (k is an integer) is designated, the EVDF at $t = t_0 + k\Delta t$ is obtained as

$$\mathbf{f}(t_0 + k\Delta t) = \mathbf{P}^k \mathbf{f}(t_0) = \left(\prod_{S=0}^{D} \mathbf{P}^{2^S b_S} \right) \mathbf{f}(t_0), \tag{30}$$

where $D = \lfloor \log_2 k \rfloor$, b_S is the Sth bit (0 or 1) in the $(D+1)$-digit binary number expression for k as $(b_D \cdots b_S \cdots b_1 b_0)_2$, and $k = \sum_{S=0}^{D} 2^S b_S$. The halfway powers must be kept in other

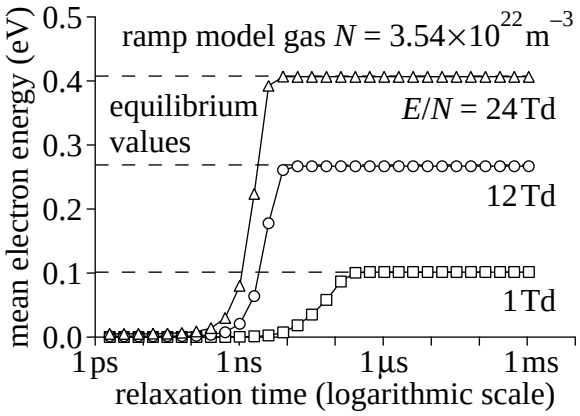

Fig. 5. Relaxation of the mean electron energy $\langle\varepsilon\rangle$ in the ramp model gas calculated by the PMPM. The time step for the original propagator matrix $\mathbf{P}$ is $\Delta t = 1\,\mathrm{ps}$.

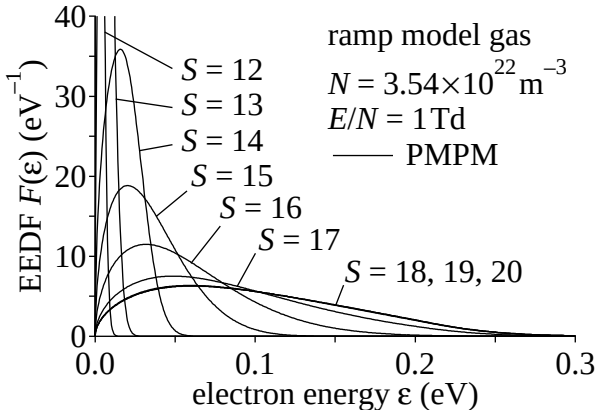

Fig. 6. Relaxation of the EEDF $F(\varepsilon)$ in the ramp model gas calculated by the PMPM. The time step for the original propagator matrix $\mathbf{P}$ is $\Delta t = 1\,\mathrm{ps}$ and S corresponds to $t = t_0 + 2^S\Delta t$.

arrays or external files if they are recalled after the matrix squaring operations up to $S = S_{\max}$, while the present PMPM proceeds as overwriting the latest $\mathbf{P}^{2^S}$ in the array having $\mathbf{P}^{2^{S-2}}$.

5. Discussion

5.1 Judgement of convergence to equilibrium solution

It is empirically believed that the equilibrium solution of the normalized EVDF is unique irrespective of the initial condition $\mathbf{f}(t_0)$. That is, for a sufficiently large $S > S_{\lim}$, normalized $\mathbf{P}^{2^S}\mathbf{f}(t_0)$ is unique for any $\mathbf{f}(t_0)$. When we choose a standard basis (unit vector) for the initial EVDF as

$$\mathbf{f}(t_0) = (\underbrace{0\ \cdots\ 0}_{s-1}\ 1\ \underbrace{0\ \cdots\ 0}_{IJ-s})^{\mathrm{T}}, \tag{31}$$

where only the sth component is unity, $\mathbf{f}(t_0 + 2^S\Delta t) = \mathbf{P}^{2^S}\mathbf{f}(t_0)$ is the sth column submatrix of $\mathbf{P}^{2^S}$ and the submatrix itself becomes the equilibrium EVDF when normalized. This applies to all s. All columns of $\mathbf{P}^{2^S}$, which can be regarded as vectors, are parallel to each other; i.e. $\mathrm{rank}(\lim_{S\to\infty}\mathbf{P}^{2^S}) = 1$, and the equilibrium EVDF is available even without the initial EVDF. This feature is known as a theorem for a stochastic matrix in a completely ergodic system, and it seems to apply also to non-conservative cases as in Ar in the presence of ionization from the uniqueness of the equilibrium EVDF. The parallelism of the columns in $\mathbf{P}^{2^S}$ could be used as a criterion for runtime judgement whether S has reached S_{lim}.

Here, $\mathbf{f}(t)$ in equilibrium is an eigenvector of $\mathbf{P}$ and its corresponding eigenvalue is $\exp(\bar{\nu}_{\mathrm{ion}}\Delta t)$ because

$$\mathbf{f}(t + \Delta t) = \mathbf{P}\mathbf{f}(t) = \exp(\bar{\nu}_{\mathrm{ion}}\Delta t)\mathbf{f}(t). \tag{32}$$

Algebraic study on $\mathbf{P}$ as an eigenvalue problem would enable us to discuss the uniqueness of the equilibrium solution or even the possibility of other types of solutions such as stationary and periodical ones as well.

5.2 Extension to dc $\mathbf{E}\times\mathbf{B}$ *model*

The PMPM is in principle applicable to the EVDF under uniform dc crossed electric and magnetic fields $\mathbf{E}\times\mathbf{B}$, because $\mathbf{P}$ in this model is time-invariant at given E/N and B/N. A difference particular to this model is only that the EVDF becomes three-variable as $f(v,\theta,\phi)$. The number of electrons $n_{i,j,k}$ in the (i,j,k)th cell $C_{i,j,k}$ is stored in a three-dimensional array, and the number of downstream neighbors of $C_{i,j,k}$ is three for regular cells or four in specific cases that the electron flow is mutual between two neighboring cells.[17,18]

A merit of the PMPM is that we can avoid a complicated optimization of the numerical relaxation sequence for $n_{i,j,k}$ discussed in a previous PM work.[18] While the relaxation is applied from the upstream cells to the downstream cells in the manner of the Gauss–Seidel method for quick convergence, the intercellular relation is cyclic and there is an exceptional region in velocity space where the direction of electron flow reverses locally against the sequential order of the cells, which makes the relaxation scheme complicated.[18]

However, the memory capacity demanded by the PMPM would limit the cell resolution. In an extreme case,[18] the total number of cells was $12000 \times 45 \times 2160$, i.e. $n \approx 9.3 \times 10^9$. It would be difficult even for the latest supercomputer to allocate an array for $\mathbf{P}$ with a size of $n \times n$ at the above n. A revolutionary extension of the memory capacity or some mathematical technique to express the EVDF finely with a reasonably small number of cells would be necessary to realize the PMPM calculation of the dc $\mathbf{E}\times\mathbf{B}$ field model.

5.3 Extension to ac **E** *model*

The PMPM is applicable also to the EVDF under uniform ac electric field $E(t)$. In this model, the EVDF can be represented in the same two-variable form as in the present dc model, and the PMPM would be applied to the propagator matrix $\mathbf{P}_T$ for whole ac period T to observe the relaxation to the periodical steady state.

Consider that T is divided into K portions of $\Delta t = T/K$. Firstly, with the propagator matrix $\mathbf{P}_k$ for the kth phase period $(k-1)\Delta t \leq t < k\Delta t$ $(1 \leq k \leq K)$, $\mathbf{P}_T$ is obtained as

$$\mathbf{P}_T = \mathbf{P}_K \cdots \mathbf{P}_2 \mathbf{P}_1. \tag{33}$$

The relaxation process in steps of T is observed by applying $\mathbf{P}_T$ to the EVDF. Secondly, the PMPM for $\mathbf{P}_T^{2^S}$ gives the relaxation for $2T$, $4T$, $8T$, $16T$, $\cdots$, $2^S T$. The EVDF at a phase in the periodical steady state would be obtained with a sufficiently large S. After that, thirdly, we may calculate the temporal variation of the EVDF within an ac period by applying $\mathbf{P}_1$ through $\mathbf{P}_K$ to the EVDF step by step again.

The computational load of this model is roughly estimated from the number of multiplication operations for the propagator matrices in addition to the size of them. The matrix multiplication is to be repeated $(2K-1)$ times in the first step to obtain $\mathbf{P}_T$ because $\mathbf{P}_k = \mathbf{P}_{\mathrm{acc},k}\mathbf{P}_{\mathrm{col}}$, S times in the second step to obtain $\mathbf{P}_T^{2^S}$, and $(K-1)$ times in the third step to obtain the EVDFs at K phases. Here, $\mathbf{P}_{\mathrm{col}}$ is time-invariant because it is independent of $E(t)$, and $K \gg S$ practically.

In the first and third steps, we may utilize the following features to reduce the number of multiplications between the matrix components and the memory capacity to hold $\mathbf{P}_{\mathrm{acc},k}$ and $\mathbf{P}_{\mathrm{col}}$. According to steps (a)–(e) explained in §3.3, $\mathbf{P}_{\mathrm{col}}$ and $\mathbf{P}_{\mathrm{acc},k}$ can be further separated as $\mathbf{P}_{\mathrm{col}} = \mathbf{P}_{\mathrm{col,out}} + \mathbf{P}_{\mathrm{col,rem}}$ and $\mathbf{P}_{\mathrm{acc},k} = \mathbf{P}_{\mathrm{acc,out},k} + \mathbf{P}_{\mathrm{acc,rem},k}$ for the electrons to move out of and remain in the source cells, respectively. $\mathbf{P}_{\mathrm{col,rem}}$ is diagonal, and $\mathbf{P}_{\mathrm{col,out}}$ is composed by rank-1 $J \times J$ submatrices because the scattering is isotropic. $\mathbf{P}_{\mathrm{acc,out},k}$ is proportional to the instantaneous value of $E(t)$ while the sign of $E(t)$ is unchanged during half an ac period, and $\mathbf{P}_{\mathrm{acc,rem},k}$ varies complementarily to $\mathbf{P}_{\mathrm{acc,out},k}$. $\mathbf{P}_{\mathrm{acc,rem},k}$ is diagonal, and $\mathbf{P}_{\mathrm{acc,out},k}$ is sparse as it has at most two non-zero components in each column. We need an efficient scheme to reproduce $\mathbf{P}_k$ by extracting necessary components from $\mathbf{P}_{\mathrm{col,out}}$, $\mathbf{P}_{\mathrm{col,rem}}$, $\mathbf{P}_{\mathrm{acc,out},k}$, and $\mathbf{P}_{\mathrm{acc,rem},k}$ stored in compressed forms.

6. Conclusions

A technology demonstration of the PMPM has been performed by calculating EVDFs under relaxation and those in equilibrium under dc electric fields. The PMPM can observe a long-term relaxation of the EVDF, and the equilibrium EVDF is also obtained successfully; the equilibrium EEDF calculated by the PMPM agreed with the results of a BE analysis and a conventional PM. In addition, theoretically possible extensions of the PMPM are discussed

for the $\mathbf{E} \times \mathbf{B}$ and ac $\mathbf{E}$ models.

On the other hand, the size of propagator matrices is limited within the memory capacity available from the present computational resources. The calculation time, which lengthens with increasing matrix size, is also a limit for practical use of the PMPM.

Nonetheless, the simplicity of its matrix-based operation is an advantage of the PMPM. The PMPM is ready to be performed by a forthcoming advanced large-scale computational platform equipped with efficient algorithm for matrix operations.

Acknowledgment This work was in part supported by KAKENHI Grant JP19K03780 from the Japan Society for the Promotion of Science.

References

1) T. Holstein, Phys. Rev. **70**, 367 (1946).
2) W. R. L. Thomas, J. Phys. B **2**, 551 (1969).
3) T. Itoh and T. Musha, J. Phys. Soc. Japan **15**, 1675 (1960).
4) R. W. L. Thomas, and W. R. L. Thomas, J. Phys. B **2** 562 (1969).
5) G. J. M. Hagelaar and L. C. Pitchford, Plasma Sources Sci. Technol. **14**, 722 (2005).
6) H. Sugawara, Plasma Sources Sci. Technol. **26**, 044002 (2017).
7) T. J. Sommerer, W. N. G. Hitchon, and J. E. Lawler, Phys. Rev. A **39**, 6356 (1989).
8) Y. A. Mankelevich, A. T. Rakhimov, and N. V. Suetin, IEEE Trans. Plasma Sci. **19**, 520 (1991).
9) H. Sugawara, Y. Sakai, and H. Tagashira, J. Phys. D **25**, 1483 (1992).
10) H. Sugawara, Y. Sakai, and H. Tagashira, J. Phys. D **27**, 90 (1994).
11) T. J. Sommerer, W. N. G. Hitchon, R. E. P. Harvey, and J. E. Lawler, Phys. Rev. A **43**, 4452 (1991).
12) W. N. G. Hitchon, G. J. Parker, and J. E. Lawler, IEEE Trans. Plasma Sci. **21**, 228 (1993).
13) G. J. Parker, W. N. G. Hitchon, and J. E. Lawler, J. Comput. Phys. **106**, 147 (1993).
14) K. Maeda and T. Makabe, Jpn. J. Appl. Phys. **33**, 4173 (1994).
15) T. Shimada, Y. Nakamura, Z. L. Petrović and T. Makabe, J. Phys. D **36**, 1936 (2003).
16) H. Sugawara and Y. Sakai, J. Phys. D **36**, 1994 (2003).
17) H. Sugawara, IEEE Trans. Plasma Sci. **47**, 1071 (2019).
18) H. Sugawara, Plasma Sci. Technol. **21**, 094001 (2019).
19) P. J. Drallos and J. M. Wadehra, J. Appl. Phys. **63**, 5601 (1988).
20) P. J. Drallos and J. M. Wadehra, Phys. Rev. A **4**, 1967 (1989).
21) K. Kitamori, H. Tagashira, and Y. Sakai, J. Phys. D **11**, 283 (1978).
22) K. Kitamori, H. Tagashira, and Y. Sakai, J. Phys. D **13**, 535 (1980).
23) H. Sugawara, H. Tagashira, and Y. Sakai, J. Phys. D **30**, 368 (1997).
24) H. Sugawara, Y. Sakai, H. Tagashira, and K. Kitamori, J. Phys. D **31**, 319 (1998).
25) H. Sugawara and Y. Sakai, J. Phys. D **32**, 1671 (1999).
26) H. Sugawara and Y. Sakai, Jpn. J. Appl. Phys. **45**, 5189 (2006).
27) D. Loffhagen and R. Winkler, J. Comput. Phys. **112**, 91 (1994).
28) D. Loffhagen and R. Winkler, J. Phys. D **29**, 618 (1996).

29) V. Strassen, Numer. Math. **13**, 354 (1969).

30) D. Coppersmith and S. Winograd, J. Symbolic Comput. **9**, 251 (1990).

31) A. Stothers, Dissertation, University of Edinburgh (2010).

32) A. M. Davie and A. J. Stothers, Proc. Royal Soc. Edinburgh **143A**, 351 (2013).

33) F. Le Gall, Proc. 39th Int. Symp. Symbolic and Algebraic Comput. (2014). https://arxiv.org/abs/1401.7714

34) I. D. Reid, Aust. J. Phys. **32** 231 (1979).

35) Y. Nakamura and M. Kurachi, J. Phys. D **21** 718 (1988).

36) K. F. Ness, J. Phys. D **27**, 1848 (1994).

37) R. D. White, M. J. Brennan, and K. F. Ness, J. Phys. D **30**, 810 (1997).